



# Physical and photophysical properties of a linear copper(I) complex of a bulky acenaphthene-based NHC ligand

Bryony M. Hockin, Campbell F. R. Mackenzie, David B. Cordes, Alexandra M. Z. Slawin, Neil Robertson & Eli Zysman-Colman

To cite this article: Bryony M. Hockin, Campbell F. R. Mackenzie, David B. Cordes, Alexandra M. Z. Slawin, Neil Robertson & Eli Zysman-Colman (2021) Physical and photophysical properties of a linear copper(I) complex of a bulky acenaphthene-based NHC ligand, Journal of Coordination Chemistry, 74:1-3, 361-379, DOI: [10.1080/00958972.2021.1871901](https://doi.org/10.1080/00958972.2021.1871901)

To link to this article: <https://doi.org/10.1080/00958972.2021.1871901>



Published online: 25 Jan 2021.



Submit your article to this journal 



Article views: 217









View related articles 



View Crossmark data 



## Physical and photophysical properties of a linear copper(I) complex of a bulky acenaphthene-based NHC ligand

Bryony M. Hockin<sup>a,b</sup> , Campbell F. R. Mackenzie<sup>a</sup> , David B. Cordes<sup>a</sup> ,  
Alexandra M. Z. Slawin<sup>a</sup> , Neil Robertson<sup>b</sup>  and Eli Zysman-Colman<sup>a</sup> 

<sup>a</sup>Organic Semiconductor Centre, EaStCHEM School of Chemistry, University of St Andrews, St Andrews, UK; <sup>b</sup>EaStCHEM School of Chemistry, University of Edinburgh, Edinburgh, UK

### ABSTRACT

We report the first example of a charge-neutral linear two-coordinate copper(I) complex bearing a sterically demanding acenaphthoimidazolylidene-based N-heterocyclic carbene (NHC) ligand. The identity and geometry of the complex are confirmed by single-crystal X-ray diffraction (XRD) analysis. The complex is poorly emissive at room temperature, showing either ligand-centered (LC) emission around 340 nm when excited at 300 nm or ligand-to-ligand charge transfer (LLCT) emission at 540 nm when excited at 420 nm; in chloroform, dual emission is observed upon photoexcitation at 300 nm. Nanosecond emission lifetimes were recorded for these processes. This is the first example of emissive linear copper(I) complexes containing this bulky NHC ligand.

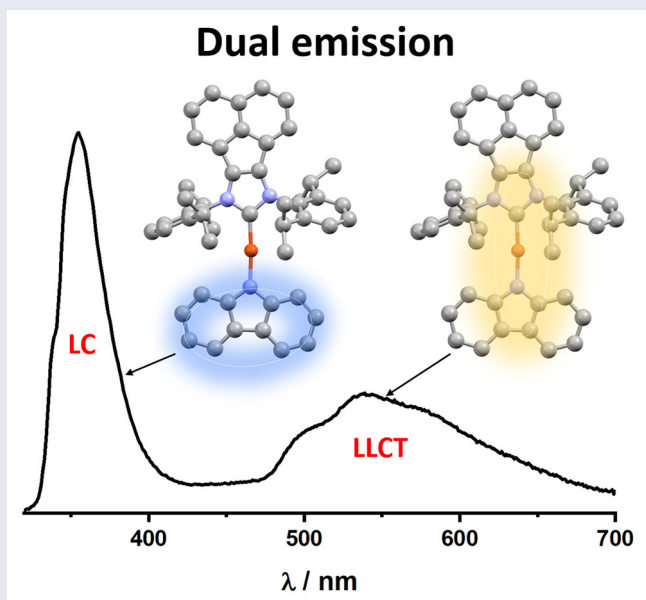
### ARTICLE HISTORY

Received 6 November 2020

Accepted 22 December 2020

### KEYWORDS

Copper complex; linear complex; acenaphthoimidazolylidene; dual emission; DFT study



**CONTACT** Eli Zysman-Colman  [eli.zysman-colman@st-andrews.ac.uk](mailto:eli.zysman-colman@st-andrews.ac.uk)  Organic Semiconductor Centre, EaStCHEM School of Chemistry, University of St Andrews, Purdie Building  North Haugh, St Andrews, KY16 9ST, UK; Neil Robertson  [neil.robertson@ed.ac.uk](mailto:neil.robertson@ed.ac.uk)  EaStCHEM School of Chemistry, University of Edinburgh, Joseph Black Building, David Brewster Rd, Edinburgh, EH9 3FJ, UK

© 2021 Informa UK Limited, trading as Taylor & Francis Group

## 1. Introduction

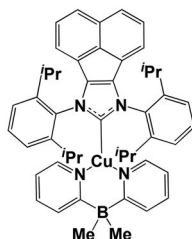
Neutral heteroleptic copper(I) complexes have long been of interest due to their favorable optoelectronic properties. This class of complexes has been used as photocatalysts [1], in biological imaging [2], and in organic light-emitting diodes (OLEDs) [3]. Most photoactive copper(I) complexes are four-coordinate with a tetrahedral geometry [4]. A major limitation of four-coordinate copper(I) emitters is the significant non-radiative decay that results from a flattening Jahn–Teller distortion of the complex in the metal-to-ligand charge transfer (MLCT) excited state, where the metal becomes formally  $d^9$  after photoexcitation [5]. This distortion also leads to ligand dissociation and solvent-induced exciplex formation, both of which adversely affect the emission by increasing non-radiative decay and decomposition rates of the complex [6]. The use of large, sterically bulky ligands that inhibit both geometric distortion in the excited state and exciplex formation, and strong  $\sigma$ -donating ligands to reduce ligand dissociation result in complexes with improved photophysical profiles [7].

Three-coordinate cationic and neutral copper(I) complexes with sterically hindered phosphine [3c,3d,8] or carbene [9] ligands tend to show high photoluminescence quantum yields ( $\Phi_{\text{PL}}$ ), emission across the visible spectrum, and display thermally activated delayed fluorescence (TADF). However, distortion in the excited state and subsequent degradation of the complex upon repeated or prolonged irradiation remains a potential problem as three-coordinate complexes undergo a Y-to-T distortion, which can lead to exciplex formation and luminescence quenching [10].

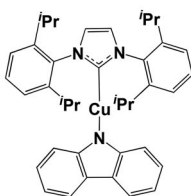
Recently, photoactive linear two-coordinate coinage metal complexes have generated much interest due to their promising photophysical properties. These complexes usually bear a neutral, bulky  $\sigma$ -donating carbene, such as a cyclic alkyl-amino carbene (CAAC) and an anionic monodentate amide ligand, such as carbazolate and do not suffer from the same distortion mechanisms as three- and four-coordinate coinage metal complexes [9c,11]. Several examples of these complexes have been used as emitters in high-performance solution-processed and vacuum-deposited OLEDs [11a,11b]. The outstanding photophysical properties of these complexes is a result of ligand-to-ligand charge transfer (LLCT), with the metal playing mostly a structural role to reduce the exchange integral between the highest occupied molecular orbital (HOMO) and lowest unoccupied molecular orbital (LUMO) involved in the transition from the low-lying excited states [12].

Relevant to this study is the neutral heteroleptic complex  $\text{Cu}(\text{IPr})(\text{Cz})$  [13], that incorporates two strongly  $\sigma$ -donating ligands: the sterically bulky N-heterocyclic carbene (NHC), 1,3-bis(2,6-diisopropylphenyl)-1,3-dihydro-2H-imidazol-2-ylidene (IPr), and carbazolate, Cz (Figure 1).  $\text{Cu}(\text{IPr})(\text{Cz})$  shows dual emission upon photoexcitation at  $\lambda_{\text{exc}} = 365$  nm in the crystalline state, with a high-energy structured fluorescence ( $\lambda_{\text{PL}}$  from 400 to 500 nm,  $\tau_{\text{PL}} = 16$  ns, 24 ns) and an oxygen-sensitive low-energy phosphorescence ( $\lambda_{\text{PL}}$  from 500 to 750 nm,  $\tau_{\text{PL}} = 55$  ms), with a corresponding photoluminescence quantum yield,  $\Phi_{\text{PL}}$ , of 33%. A second, more recent study of the related neutral  $\text{Cu}(\text{PyTz})(\text{Cz})$  complexes (PyTz = 2-methyl-[1,2,3]triazolopyridine) reported LLCT emission between Cz and PyTz that was assigned as TADF with lifetimes in the crystalline state of 0.6  $\mu\text{s}$  for  $\text{Cu}(\text{PyTz})(\text{Cz})$  [14]. Additionally, in THF solution, these complexes form a monomer-dimer equilibrium and as a result exhibit dual-emission with bands at 437 and 594 nm [14].

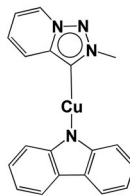
## Previous work:



**Cu(IPrBIAN)(py<sub>2</sub>BMe<sub>2</sub>)**  
 $\lambda_{\text{PL}} \sim 610 \text{ nm}$   
 $\tau_{\text{PL}} < 10 \text{ ns}$   
 (THF glass, 77 K)

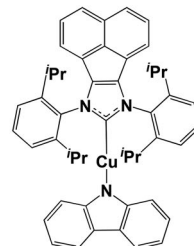


**Cu(IPr)(Cz)**  
 $\lambda_{\text{F}} = 400\text{--}500 \text{ nm}$ ,  
 $\tau_{\text{F}} = 16, 24 \text{ ns}$   
 $\lambda_{\text{ph}} = 500\text{--}750 \text{ nm}$ ,  $\tau_{\text{ph}} = 55 \text{ ms}$   
 ( $\lambda_{\text{exc}} = 365 \text{ nm}$ , crystal, RT)



**Cu(PyTz)(Cz)**  
 $\lambda_{\text{PL}} = 437 \text{ \& } 594 \text{ nm}$   
 $\tau_{\text{PL}} = 4.4 \text{ ns}$   
 ( $\lambda_{\text{exc}} = 375 \text{ nm}$ , THF, RT)

## This work:



**3: Cu(IPrBIAN)(Cz)**  
 $\lambda_{\text{PL}} = 390 \text{ nm}$ ,  $\tau_{\text{PL}} = 1.6, 4.8 \text{ ns}$   
 $\lambda_{\text{PL}} = 550 \text{ nm}$ ,  $\tau_{\text{PL}} = 1.4, 7.4 \text{ ns}$   
 ( $\lambda_{\text{exc}} = 300 \text{ nm}$ , CHCl<sub>3</sub>, RT)

**Figure 1.** Previous work on 2- and 3-coordinate copper(I) complexes, Cu(IPrBIAN)(py<sub>2</sub>BMe<sub>2</sub>) [9b], Cu(IPr)(Cz) [13], and Cu(PyTz)(Cz) [14] along with synthetic target 3.

A bulkier and more  $\pi$ -accepting analog of IPr is IPrBIAN (**1**), which has been used as a ligand in a number of complexes of silver, gold [15], palladium [16], iridium [17], and ruthenium [18]. The application of these complexes has been in catalysis; palladium complexes of IPrBIAN have been used as mild catalysts for aminocarbonylation of iodarenes [16a], for Negishi couplings [16b] and Suzuki–Miyaura couplings with sterically hindered substrates [16c], while Hoveyda II-type Ru complexes using IPrBIAN ligands have been used for ring-closing metathesis [18]. There is only one reported example of a copper(I) complex using IPrBIAN as a ligand (Figure 1) [9b]. The three-coordinate Cu(IPrBIAN)(py<sub>2</sub>BMe<sub>2</sub>) complex was found to be non-emissive in the solid state at room temperature and only showed weak, structured ligand-centered (LC) emission ( $\lambda_{\text{PL}} \sim 610 \text{ nm}$ ,  $\Phi_{\text{PL}} < 1\%$ ,  $\tau_{\text{PL}} < 10 \text{ ns}$ ) in a 2-methyltetrahydrofuran glass at 77 K.

In this work, we report the first example of a neutral linear two-coordinate Cu(I) complex Cu(IPrBIAN)(Cz) (**3**) bearing an IPrBIAN NHC ligand. As with the analogous Cu(IPr)(Cz), it also exhibits dual emission, but in chloroform solution rather than the solid state [13, 14].

## 2. Experimental

### 2.1. Chemical and starting materials

All reagents and solvents were of reagent grade for synthesis, spectroscopic grade for analysis, and were used as supplied.

### 2.2. Instrumentation

#### 2.2.1. Purification, NMR spectroscopy, melting point determination, and mass spectrometry

All reactions were performed using standard Schlenk techniques under an inert (N<sub>2</sub>) atmosphere. Flash column chromatography was performed using silica gel (Silica-P from Silicycle, 60 Å, 40–63 mm). Analytical thin-layer chromatography was performed

on silica plates with aluminum backings (250 mm with indicator F-254). Compounds were visualized under UV light. Nuclear magnetic resonance (NMR) spectra were recorded in  $\text{CDCl}_3$  at room temperature (r.t.) on a Bruker AV400 or AV 500 spectrometer at 400 MHz for  $^1\text{H}$  NMR and at 101 MHz for  $^{13}\text{C}$  NMR, respectively. Chemical shifts are reported in parts per million (ppm) relative to TMS and calibrated using the respective residual solvent signals. Melting and decomposition points were determined by heated solid samples in sealed glass capillaries using a Stuart SMP 30 melting point apparatus and are uncorrected. High-resolution nano-spray ionization (NSI) mass spectra were collected on a Waters Xevo QTOF instrument by the EPSRC National Mass Spectrometry Service Centre (NMSSC), Swansea. High-resolution electro-spray ionization (ESI) mass spectra were collected on a Bruker MicroTOF 2 instrument by Alan Walker at the University of Edinburgh.

### 2.2.2. Cyclic voltammetry and differential pulse voltammetry

Cyclic voltammetry (CV) analysis was performed on a  $\mu\text{AUTOLAB}$  Type III potentiostat at a sweep rate of  $100 \text{ mV s}^{-1}$ . Differential pulse voltammetry (DPV) was conducted with an increment potential of  $0.004 \text{ V}$  and a pulse amplitude of  $50 \text{ mV}$ , width of  $0.05 \text{ s}$ , and period of  $0.5 \text{ s}$ . Samples were prepared as  $0.6 \text{ mM}$  dichloromethane (DCM) solutions, which were degassed by sparging with DCM-saturated nitrogen gas for  $5 \text{ min}$  prior to measurements. All measurements were performed using  $0.1 \text{ M}$  DCM solution of tetra-*n*-butylammonium hexafluorophosphate ( $[\text{nBu}_4\text{N}]\text{PF}_6$ ). An  $\text{Ag}/\text{Ag}^+$  electrode was used as the reference electrode while a glassy carbon electrode and a platinum rod were used as the working electrode and counter electrode, respectively. The redox potentials are reported relative to a saturated calomel electrode (SCE) with a ferrocene/ferrocenium ( $\text{Fc}/\text{Fc}^+$ ) redox couple as the internal standard ( $0.46 \text{ V}$  vs. SCE in DCM) [19].

### 2.2.3. UV-vis absorption spectroscopy

Electronic spectra were recorded using a Jasco V-670 UV/vis/NIR spectrophotometer controlled with SpectraManager software (compounds **1H.CI** and **2**) or a Shimadzu UV-2600 UV spectrophotometer (**3**). All samples were prepared in DCM, chloroform or toluene with varying concentrations in the order of  $\text{mM}$ . Molar absorptivity determination was verified by linear least-squares fit of values obtained from at least four independent solutions at varying concentrations (for DCM:  $0.037$ – $0.18 \text{ mM}$ ; for chloroform:  $0.012$ – $0.054 \text{ mM}$ ; for toluene:  $0.034$ – $0.17 \text{ mM}$ ).

### 2.2.4. Steady-state and time-resolved emission spectroscopy

The sample solutions for emission measurements were prepared in toluene, DCM, THF, or chloroform, with concentrations between  $20$  and  $80 \mu\text{M}$ , and degassed using three cycles of freeze-pump-thaw technique using an in-house designed quartz cuvette. Steady-state emission spectra and excitation spectra were recorded using an Edinburgh Instruments F980 fluorimeter. Excited-state lifetimes were measured by the time-correlated single-photon counting (TCSPC) technique using an Edinburgh Instruments F980 fluorimeter equipped with a pulsed diode laser (exciting at  $378 \text{ nm}$ ); PL emission was detected at  $390 \text{ nm}$  (LC emission) or  $550 \text{ nm}$  (CT emission).

**Table 1.** Selected crystallographic data for **1H.Cl**, **2**, and **3**.

Compound	<b>1H.Cl</b> •1.5CH <sub>2</sub> Cl <sub>2</sub>	<b>2</b>	<b>3</b>
CCDC	2,038,660	2,038,661	2,038,662
Formula	C <sub>38.5</sub> H <sub>44</sub> Cl <sub>4</sub> N <sub>2</sub>	C <sub>37</sub> H <sub>40</sub> ClCuN <sub>2</sub>	C <sub>49</sub> H <sub>48</sub> CuN <sub>3</sub>
Mw (g mol <sup>-1</sup> )	676.60	611.74	742.48
Crystal description	Yellow prism	Yellow prism	Yellow plate
Crystal size [mm <sup>3</sup> ]	0.20 × 0.07 × 0.03	0.12 × 0.04 × 0.03	0.27 × 0.12 × 0.02
Space group	Pnma	C2/c	P2/c
<i>a</i> [Å]	24.722 (3)	32.5243 (9)	19.9728 (5)
<i>b</i> [Å]	17.017 (2)	27.2274 (8)	8.6927 (2)
<i>c</i> [Å]	18.298 (2)	32.8590 (9)	23.2178 (6)
$\beta$ [°]	90.00	90.440 (2)	90.744 (3)
Vol [Å <sup>3</sup> ]	7697.9 (15)	29097.5 (14)	4030.68 (17)
Z	8	32	4
$\rho$ (calc) [g cm <sup>-3</sup> ]	1.168	1.117	1.223
$\mu$ [mm <sup>-1</sup> ]	0.334	0.698	0.579
F(000)	2856	10304	1568
Reflections collected	91939	193229	50753
Independent reflections ( <i>R</i> <sub>int</sub> )	7311 (0.0911)	34205 (0.1243)	9302 (0.0466)
Parameters, restraints	454, 28	1515, 96	591, 48
GoF on <i>F</i> <sup>2</sup>	1.027	0.978	1.059
<i>R</i> <sub>1</sub> [ <i>I</i> > 2 $\sigma$ ( <i>I</i> )]	0.0686	0.0756	0.0532
<i>wR</i> <sub>2</sub> (all data)	0.2153	0.2257	0.1314
Largest diff. peak/hole [e/Å <sup>3</sup> ]	0.71, -0.45	0.96, -0.62	0.42, -0.47

### 2.3. X-ray crystallography

X-ray diffraction (XRD) data for all compounds were collected at 173 K using a Rigaku FR-X Ultrahigh Brilliance Microfocus RA generator/confocal optics with an XtaLAB P200 diffractometer [Mo K $\alpha$  radiation ( $\lambda = 0.71075$  Å)]. Intensity data were collected using  $\omega$  steps accumulating area detector images spanning at least a hemisphere of reciprocal space. Data for all compounds analyzed were collected using CrystalClear [20] and processed (including correction for Lorentz, polarization, and absorption) using either CrystalClear or CrysAlisPro [21]. Structures were solved by direct (SIR2004) [22] or dual-space (SHELXT) [23] methods and refined by full-matrix least-squares against *F*<sup>2</sup> (SHELXL-2018/3) [24]. Non-hydrogen atoms were refined anisotropically, and hydrogen atoms were refined using a riding model. Compound **3** was twinned with a twin law of  $-1\ 0\ 0\ 0\ -1\ 0\ 0\ 0\ 1$  and a refined twin fraction of 0.15. Both **1H.Cl** and **2** showed void space containing poorly ordered solvent (**1H.Cl**: 215 Å<sup>3</sup>, **2**: 4291 Å<sup>3</sup>) and the SQUEEZE [25] routine implemented in PLATON [26] was used to remove the contribution to the diffraction pattern of the unordered electron density in the void spaces. All calculations except SQUEEZE were performed using the CrystalStructure [27] interface. Selected crystallographic data are presented in Table 1. Deposition numbers 2,038,660–2,038,662 contain the supplementary crystallographic data for this article. These data are provided free of charge by the joint Cambridge Crystallographic Data Centre and Fachinformationszentrum Karlsruhe Access Structures service ([www.ccdc.cam.ac.uk/structures](http://www.ccdc.cam.ac.uk/structures)).

### 2.4. Synthesis of complexes

*Bis*(2,6-(diisopropyl)phenyl)acenaphthylene-1,2-diimine: To a two-neck round bottom flask equipped with a reflux condenser under nitrogen was added acenaphthenequinone (1.35 g, 7.40 mmol, 1 equiv.) in acetonitrile (65 mL) and the solution was refluxed for 45 min. Acetic acid (12 mL) was then added and stirring continued until the total

dissolution of acenaphthenequinone. 2,6-diisopropylaniline (2.84 g, 16 mmol, 2 equiv.) was added dropwise. The solution was heated at reflux for 5 h and then cooled to room temperature. The precipitate was filtered and washed with hexane. After air-drying, the product was obtained as an orange powder. **Mass:** 2.977 g. **Yield:** 80%. **Mp:** 316–320 °C. **<sup>1</sup>H NMR (400 MHz, CDCl<sub>3</sub>) δ (ppm):** 7.87 (d, *J* = 8.24 Hz, 2H), 7.35 (t, *J* = 7.92 Hz, 2H), 7.29–7.22 (m, 6H), 6.63 (d, *J* = 7.20 Hz, 2H), 3.03 (h, *J* = 6.96 Hz, 4H), 1.23 (d, *J* = 6.84 Hz, 12H), 0.97 (d, *J* = 6.96 Hz, 12H). **<sup>13</sup>C NMR (101 MHz, CDCl<sub>3</sub>) δ (ppm):** 160.80, 147.28, 147.00, 135.26, 132.00, 129.30, 129.17, 128.72, 128.10, 127.93, 127.71, 124.81, 124.13, 123.29, 123.23, 123.18, 122.05, 28.43, 28.17, 23.25, 22.95, 22.68. **HR-MS (NSI):** Calculated for [M + H]<sup>+</sup>(C<sub>36</sub>H<sub>41</sub>N<sub>2</sub>): 501.3270 *m/z* Found [M + H]<sup>+</sup>: 501.3270 *m/z*. Characterization matches that previously reported [28].

*7,9-bis(2,6-diisopropylphenyl)-7H-acenaphtho[1,2-d]imidazol-9-ium chloride, 1H.Cl:* To a nitrogen-flushed thick-walled reaction vessel was added bis(2,6-(diisopropyl)phenyl)acenaphthylene-1,2-diimine (0.500 g, 1.0 mmol, 1 equiv.) under nitrogen. Methoxymethyl chloride (MOMCl, 1.5 mL, 20 mmol, 20 equiv.) was added and the reaction was heated at 100 °C with stirring for 16 h. After cooling to room temperature, 10 mL of diethyl ether was added and a yellow precipitate formed. The precipitate was filtered and washed with diethyl ether to give the product, which was dried under vacuum. Residual MOMCl waste was quenched with aqueous ammonia. The product was isolated as a yellow powder. **Mass:** 0.410 g. **Yield:** 70%. **Mp:** 349–352 °C. **<sup>1</sup>H NMR (400 MHz, CDCl<sub>3</sub>) δ (ppm):** 12.10 (s, 1H), 8.02 (d, *J* = 8.04 Hz, 2H), 7.69 (t, *J* = 7.88 Hz, 2H), 7.60 (dd, *J* = 8.30, 7.12 Hz, 2H), 7.49 (d, *J* = 7.84 Hz, 4H), 7.23–7.21 (m, 2H), 2.73 (h, *J* = 6.84 Hz, 4H), 1.43 (d, *J* = 6.84 Hz, 12H), 1.18 (d, *J* = 6.84 Hz, 12H). **<sup>13</sup>C NMR (101 MHz, CDCl<sub>3</sub>) δ (ppm):** 135.89, 129.32, 128.33, 124.75, 123.93, 123.81, 69.31, 29.09, 23.89, 23.60. **HR-MS (NSI):** Calculated for [M]<sup>+</sup>(C<sub>37</sub>H<sub>41</sub>N<sub>2</sub>): 513.3270 *m/z* Found [M]<sup>+</sup>: 513.3262 *m/z*. Characterization matches that previously reported [28].

*(7,9-bis(2,6-diisopropylphenyl)-7H-acenaphtho[1,2-d]imidazol-9-ium)copper(I) chloride, 2:* To a nitrogen flushed 100 mL RBF were added **1H.Cl** (400 mg, 0.720 mmol, 1 equiv.), CuCl (85.0 mg, 0.863 mmol, 1.2 equiv.), NaO<sup>t</sup>Bu (0.069 g, 0.72 mmol, 1 equiv.) and dry THF (60 mL). The cloudy orange solution was stirred overnight under nitrogen during which it turned colorless. The solution was exposed to air, filtered through a celite plug and the solvent removed under reduced pressure. To the residue was added toluene (30 mL) and the solution was filtered again, and the filtrate collected. The solvent was evaporated to give the product as a yellow solid. **Mass:** 0.425 g. **Yield:** 80%. **Mp:** 270–276 °C. **<sup>1</sup>H NMR (400 MHz, CDCl<sub>3</sub>) δ (ppm):** 7.80 (dd, *J* = 8.40, 0.64 Hz, 2H), 7.59 (t, *J* = 7.80 Hz, 2H), 7.45–7.40 (m, 6H), 7.18–7.16 (m, 2H), 2.84 (h, *J* = 6.88 Hz, 4H), 1.35 (d, *J* = 6.88 Hz, 12H), 1.15 (d, *J* = 6.84 Hz, 12H). **<sup>13</sup>C NMR (101 MHz, CDCl<sub>3</sub>) δ (ppm):** 145.70, 130.95, 128.46, 127.95, 124.66, 121.14, 29.07, 25.02, 23.89. **HRMS (ESI):** Calculated [M]<sup>+</sup>(C<sub>37</sub>H<sub>40</sub>N<sub>2</sub>CuCl): 610.2176 *m/z* (M + ion not observed). Calculated [M + 2H-CuCl]<sup>+</sup>(C<sub>37</sub>H<sub>42</sub>N<sub>2</sub>): 514.3343 Found [M + 2H-CuCl]<sup>+</sup>: 514.3334 *m/z*. Characterization matches that previously reported [9b].

*Copper(I) (7,9-bis(2,6-diisopropylphenyl)-7H-9H-acenaphtho[1,2-d]imidazol-8-yl)(9H-carbazol-9-yl), [Cu(IPrBIAN)(cz)], 3:* To a solution of **2** (180 mg, 0.290 mmol, 1 equiv.) in DCM (25 mL) was added carbazole (49.2 mg, 0.290 mmol, 1 equiv.), NaOH (1 mL, 0.5 M solution), and Bu<sub>4</sub>NCl (8.0 mg, 0.03 mmol, 0.1 equiv.). The solution was stirred for 48 h



during which a color change from yellow to orange was observed. Fifty milliliter of water was added, and the solution stirred for 1 h. The aqueous layer was extracted three times with DCM (50 mL) and the solvent removed under reduced pressure to give an orange solid. This was recrystallized from DCM/hexane, filtered and washed with hexane to give the product as orange needles (**Mass**: 0.126 g). **Yield**: 58%. **Mp**: >300 °C. **<sup>1</sup>H NMR (400 MHz, CDCl<sub>3</sub>) δ (ppm)**: 8.08 (d, *J* = 7.08 Hz, 2H), 7.92 (d, *J* = 7.60 Hz, 2H), 7.84 (d, *J* = 8.20 Hz, 2H), 7.81–7.74 (m, 3H), 7.59–7.50 (m, 6H), 7.49–7.39 (m, 6H), 7.18 (d, *J* = 7.0 Hz, 2H), 7.01–6.98 (m, 3H), 6.88 (t, *J* = 7.20 Hz, 2H), 6.37 (d, *J* = 8.10 Hz, 2H), 2.98 (h, *J* = 6.90 Hz, 4H), 1.31 (d, *J* = 6.90 Hz, 12H), 1.18 (d, *J* = 6.90 Hz, 12H). **<sup>13</sup>C NMR (101 MHz, CDCl<sub>3</sub>) δ (ppm)**: 146.31, 145.71, 130.95, 128.47, 128.03, 125.95, 124.66, 123.23, 121.23, 120.45, 119.55, 115.10, 114.46, 110.72, 29.06, 25.00, 23.88, 1.17. **HRMS (ESI)**: Calculated [M]<sup>+</sup> (C<sub>49</sub>H<sub>48</sub>N<sub>3</sub>Cu): 741.3150 *m/z* Found [M]<sup>+</sup>: 741.3198 *m/z*.

## 2.5. Density functional theory (DFT) studies

Density functional theory (DFT) calculations were performed using the Gaussian 09 (Rev. D.01; Gaussian Inc., Wallingford, CT) [29] suite of software. All calculations were performed using the B3LYP functional [30] and the 6–31 G(d,p) basis set [31] for non-metal atoms and the SBKJC VDZ ECP basis set [32] for Cu atoms, using the conductor-like polarizable continuum model (CPCM) [33] for DCM solution. Singlet ground state geometry optimizations were carried out using crystallographic structures as starting points; vibrational frequency calculations were performed to ensure that the optimized geometries represented the local minima. Geometry optimization of the triplet state was performed using the optimized singlet structure as the starting point. Excited-state energies were calculated using the TD-DFT formalism at the same level of theory [34].

Calculated structures and Kohn-Sham orbitals were visualized with Gaussview version 5.0 (Semichem Inc., Shawnee, KS) [35]. Chemissian version 4.60 (Lenoid Skripnikov, St. Petersburg, Russia) [36] was used to calculate and visualize the fractional contributions of various groups to each molecular orbital. GaussSum version 2.2 (Noel O'Boyle, Dublin, Ireland) [37] was used to calculate and visualize UV–vis spectra and oscillator strength.

## 3. Results and discussion

### 3.1. Synthesis and characterization of the precursors and copper complexes

IPrBIAN synthesis proceeded without the requirement for the commonly used ZnCl<sub>2</sub> templating agent [38]. The IPrBIAN imidazolium salt 1H.Cl was synthesized from IPrBIAN in good yields using a solvent-free procedure adapted from the literature; addition of diethyl ether afforded the product as a yellow powder [39]. The complexation of this pro-ligand 1H.Cl to copper(I) chloride proceeded using sodium *tert*-butoxide at room temperature to afford the desired [Cu(IPrBIAN)Cl] complex 2 in good yield (Figure 2)

Substitution of the chlorido ligand with carbazolate proceeded in reasonable yield under basic conditions and in the presence of tetrabutylammonium chloride as a phase transfer catalyst to afford [Cu(IPrBIAN)(Cz)], **3**, as an orange powder [40]. Pro-



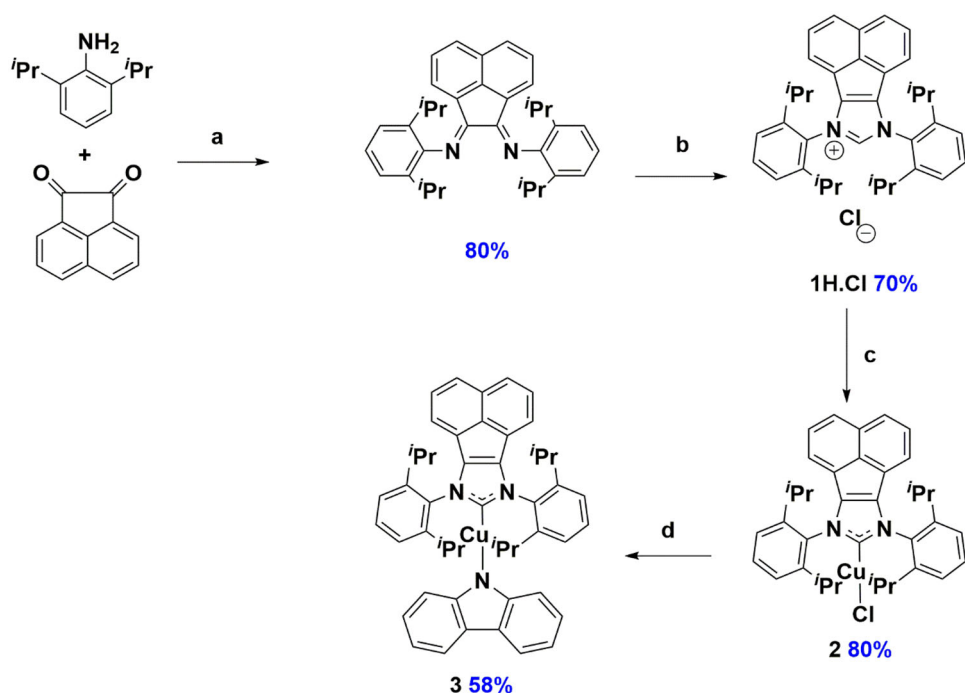


**Figure 2.** Synthesis of NHC ligands and 1–3. Reagents and conditions: <sup>a</sup>MeCN, AcOH, 80 °C, 5 h; <sup>b</sup>MOMCl (40 mmol), 100 °C, 16 h; <sup>c</sup>CuCl (1 equiv.), NaO<sup>t</sup>Bu (2 equiv.), THF, r.t., 24 h. <sup>d</sup>Carbazole, NaOH (0.5 M, 2 mL), Bu<sub>4</sub>NCl, DCM, 48 h, r.t.

ligand **1H.Cl** and complexes **2** and **3** were characterized by <sup>1</sup>H and <sup>13</sup>C NMR spectroscopy, melting point determination, HR ESI-MS, and single-crystal XRD analysis.

### 3.2. Solid-state structures

Yellow crystals of **1H.Cl** and **2** were obtained by slow diffusion of diethyl ether into a solution of **1H.Cl** in MeCN; or pentane into a solution of **2** in DCM. Orange crystals of **3** were obtained by slow diffusion of pentane into a solution of **3** in DCM. Crystal structures of **1H.Cl** and **2** are shown in Figure 3 while the crystal structure of **3** is shown in Figure 4. The structure of **2** shows very slight distortion from linearity at the copper, with a bond angle of 177.50(2)°.

Complex **3** shows a similar, slight distortion from linearity with a C1–Cu1–N52 bond angle of 176.39(10)°, and the C1–Cu bond lengths do not vary significantly between **2** and **3**, at 1.851(6) and 1.864(2) Å, respectively. The related complex Cu(IPr)(Cz) has a slightly longer Cu–C bond distance of 1.877(2) Å [13], suggesting that the acenaphthene backbone present on **2** and **3** slightly increases the carbene σ-donation and strengthens the Cu–C<sub>carbene</sub> bond. In **3** the IPrBIAN and Cz ligands are nearly co-planar, with an angle between the IPrBIAN and Cz planes of 7.65°. Literature examples of linear Cu(NHC)(Cz) complexes exhibit a range of angles between the NHC and Cz ligands, from orthogonal in Cu(IPr)(Cz) (IPr–Cz plane angle is 89.9°) [13], to almost co-planar in Cu(PyTz)(Cz) (PyTz–Cz plane angle is 5.9°) [14], with an intermediate value of 33.9° observed for Cu(IMes)(Cz) [13].

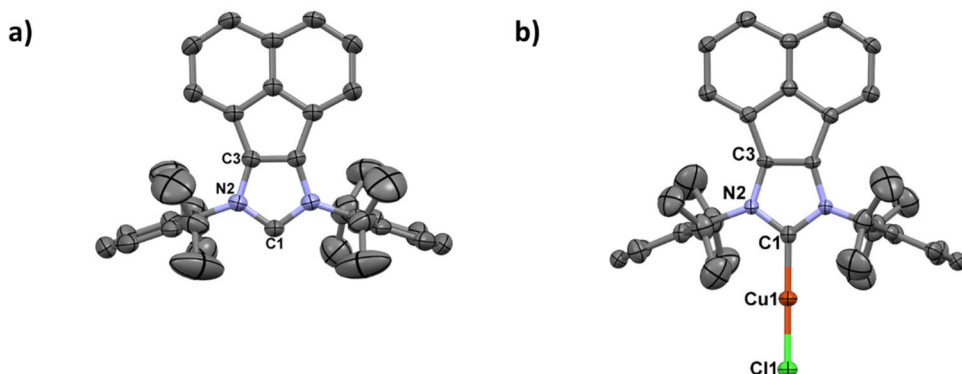


**Figure 3.** Molecular structure of (a) one independent cation of **1H.Cl** and (b) one independent molecule of **2**. Solvent and hydrogen atoms have been omitted for clarity. Thermal ellipsoids are drawn at the 50% probability level.

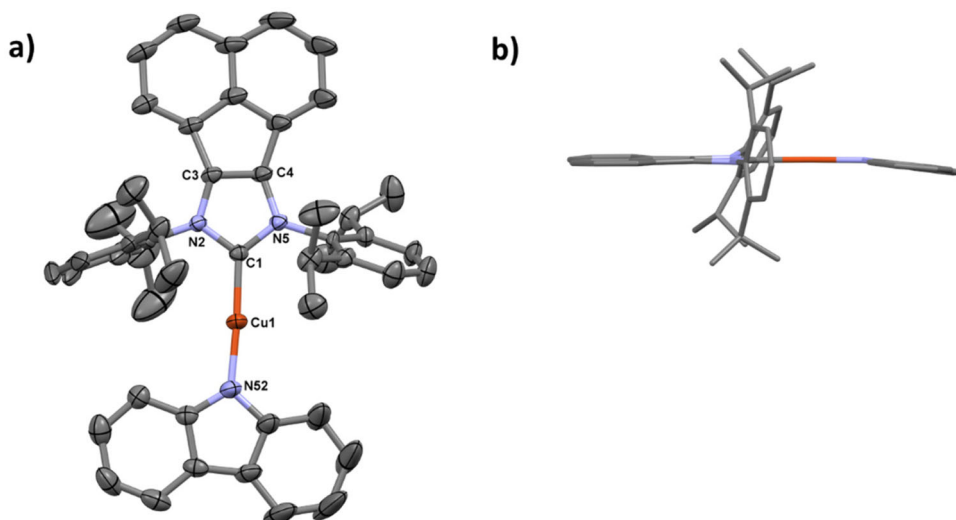


**Figure 4.** Views of the structure of **3**, Cu(IPrBIAN)(Cz). (a) Thermal ellipsoid plot, ellipsoids are drawn at the 50 % probability level. (b) Side view of a wireframe representation of the structure. Hydrogens and the minor component of the disorder have been omitted for clarity.

A key difference between the predicted and the observed structures is the uneven copper-NHC bond angles in the crystal structure; the angle N2–C1–Cu1 [ $124.7(2)^\circ$ ] differs noticeably from N5–C1–Cu1 [ $130.1(2)^\circ$ ], resulting in a slightly skewed orientation of the NHC relative to the predicted structure (where the two angles are the same). This skewing of the NHC in the crystal structure such that the *i*Pr groups on one side of the complex show greater proximity to the Cz than the other is likely due to crystal packing. Apart from this discrepancy in NHC orientation, the observed bond lengths and angles match well with those predicted by DFT (Table 2).

**Table 2.** Comparison of observed bond distances and angles for **3** with values calculated for **3**.

Bond lengths (Å)			Bond angles (°)		
	Obs. (X-ray)	Calcd. (DFT)		Obs. (X-ray)	Calcd. (DFT)
Cu1–C1	1.864 (2)	1.864	C1–Cu1–N52	176.39 (10)	179.99
Cu1–N52	1.8540 (19)	1.855	N2–C1–Cu1	124.74 (16)	127.23
N52–C53	1.376 (3)	1.384	N5–C1–Cu1	130.12 (16)	127.23
N52–C64	1.375 (3)	1.384	C64–N52–Cu1	126.34 (16)	126.69
C1–N2	1.365 (3)	1.370	C53–N52–Cu1	126.83 (18)	126.69
C1–N5	1.370 (3)	1.370	C1–N5–C28	121.9 (8)	122.36
N2–C3	1.371 (3)	1.381	C1–N2–C16	123.68 (18)	122.36
N5–C4	1.387 (3)	1.381	NHC–Cz <sup>a</sup>	7.65	4.35
C3–C4	1.353 (3)	1.380	Cu–Cz <sup>b</sup>	6.8 (5)	0
N2–C16	1.441 (3)	1.438	–	–	–
N5–C28	1.549 (16)	1.438	–	–	–

<sup>a</sup>The angle between the NHC plane and the Cz plane. <sup>b</sup>Cu1–N52–C53–C54 Torsion angle.

### 3.3. DFT and TD-DFT calculations

DFT and time-dependent DFT (TD-DFT) calculations of **2** and **3** were undertaken to provide insight into ground and excited-state properties. The optimized ground state structure of **2** matches well with the observed crystal structure. The HOMO is distributed mostly on the IPrBIAN ligand (87%) and the copper (10%), with the LUMO localized solely on the IPrBIAN (100%); the corresponding HOMO–LUMO gap is 3.12 eV. According to TD-DFT most of the transitions possessing a strong oscillator strength ( $f > 0.02$ ) originate from LC transitions of the IPrBIAN and a small contribution from copper to IPrBIAN MLCT (Table 3). The first three transitions ( $S_1$ ,  $S_2$ , and  $S_3$ ) correspond to the lowest energy absorption band and are assigned as HOMO→LUMO, H-1→LUMO, and H-2→LUMO, respectively. All of these transitions have major IPrBIAN-centered intra-ligand CT character; the  $S_2$  transition also has some minor Cu ( $d\pi$ ) → IPrBIAN ( $\pi^*$ ) MLCT character.

Two optimized structures were obtained for **3**. The lowest-energy conformer has the IPr(BIAN) and Cz ligands almost co-planar (angle between the mean-planes of the two ligands is 4.35°), similar to the geometry observed in the X-ray structure (angle between mean-planes of 7.65°). The second, higher energy, conformer (12 kJ mol<sup>−1</sup> destabilized) has the two ligands orthogonal to each other (angle of rotation between the two ligands is 89.66°). These results are in contrast to calculations conducted on other linear (NHC)–Cu–Cz complexes in which the lowest energy calculated structures dispose the NHC and Cz ligands orthogonal to each other [13]. From TD-DFT calculations, Li *et al.* concluded that the nonplanar geometry between the carbene and the Cz weakens the charge transfer character and that the emission becomes almost entirely LC in nature, whereas in the case of **3**, the weak emission at 550 nm can be assigned to originating from a LLCT state. A rigid potential energy scan (PES) of the angles between the IPrBIAN and Cz ligands in **3** (Figure 5(a)) revealed an energy barrier to interconversion between the two conformers of approximately 23 kJ mol<sup>−1</sup>. Given the energy difference between the two conformers and the rotational barriers, it is expected that the compound will exist only in the lower energy co-planar conformation. Excited state calculations (TD-DFT and triplet structure optimization) were thus performed using the lower energy co-planar conformation of **3**.

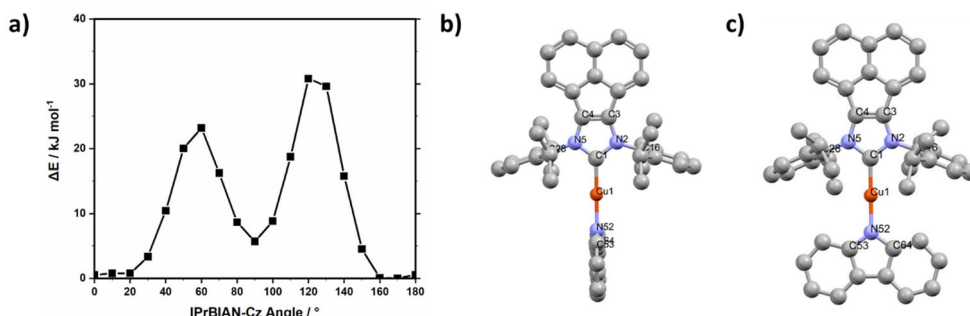


**Figure 5.** a) Rigid potential angle energy scan of **3**; the optimized geometry of the orthogonal structure was used as the starting point, with the angle between the IPrBIAN and Cz ligands rotated through  $180^\circ$  in  $10^\circ$  steps. Representation of the two optimized ground state structures observed; b) higher energy orthogonal conformation; c) lower energy co-planar conformation.

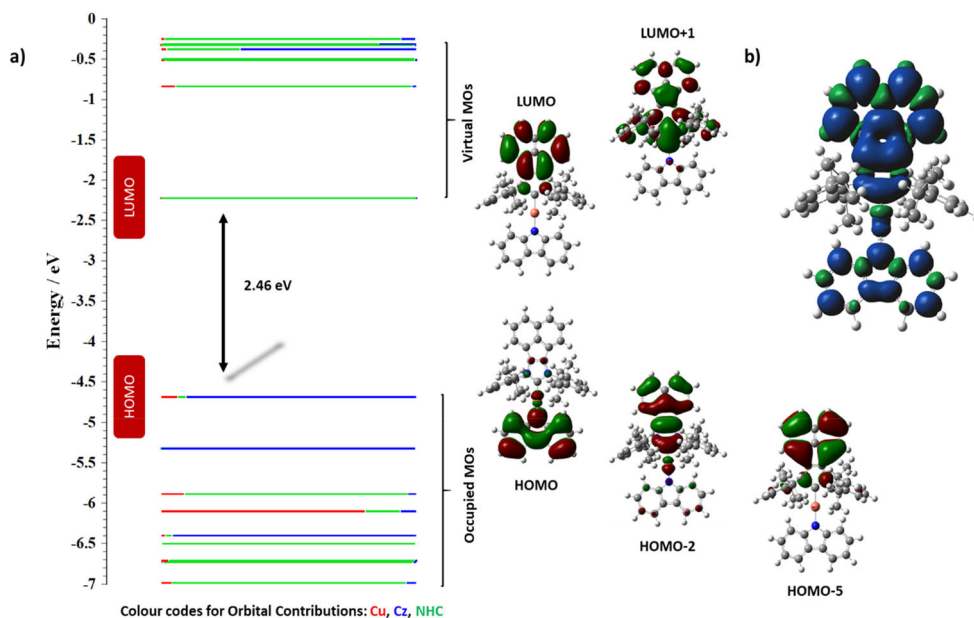


**Figure 6.** Summary of DFT calculations of **3**. a) Energy level diagram calculated using DFT using B3LYP/SBKJC-VDZ ECP for the Cu(I) center and 6-31G\*\* for the atoms C, H, and N with CPCM( $\text{CH}_2\text{Cl}_2$ ) and a 0.5 eV threshold of degeneracy (isocontour of 0.03), showing HOMO-2, HOMO, LUMO, and LUMO + 1 orbitals of **3**. b) Triplet spin density of **3** (isocontour of 0.02).

In the ground state, the HOMO of **3** is distributed mostly on the carbazolate ligand (94%) with a minor contribution from the copper center (5%), while the LUMO is localized on the naphthalene moiety of the IPrBIAN (100%) (Figure 6(a)). The calculated HOMO-LUMO gap is 2.46 eV. The relative LUMO energies of **2** and **3** are similar (−2.44 and −2.23 eV, respectively), with the substitution of the chlorido ligand for the more strongly  $\sigma$ -donating carbazolate ligand in **3** resulting in a destabilization of the LUMO.

According to TD-DFT, and in agreement with literature studies of the related complex Cu(IPr)(Cz) [13], most of the transitions with a strong oscillator strength ( $f > 0.02$ )

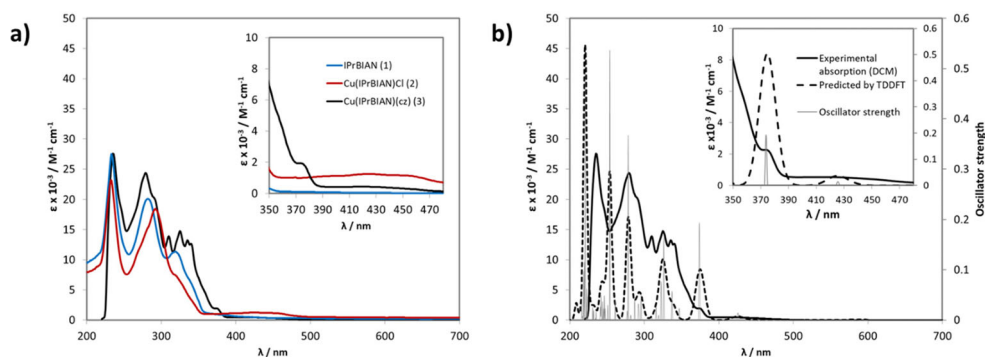


**Figure 7.** a) Absorption spectra of solutions of **1H.Cl** (blue line), **2** (red line) and **3** (black line) in dichloromethane. b) Experimental absorption spectra (solid lines) of solutions of **3** in DCM. Spectra predicted by TD-DFT in DCM shown as dashed lines; predicted oscillator strength for each transition shown as grey lines.

originate from LC transition of the Cz. However, unlike previous examples of two-coordinate copper(I) complexes [11c], the oscillator strength of the  $S_1$  transition is very small ( $f=0.0015$ ). The calculated  $S_1$  and  $T_1$  energies for **3** are 2.122 and 2.027 eV, respectively, resulting in a singlet-triplet energy gap,  $\Delta E_{ST}$  of 95 meV. The small  $\Delta E_{ST}$ , reflective of the CT character of the  $S_1$  and  $T_1$  states, implies that this compound should exhibit TADF [41]. Indeed, the  $S_1$  state can best be described as a LLCT between Cz and IPrBIAN (HOMO $\rightarrow$ LUMO, 99%). The first singlet excited state with a significant oscillator strength is  $S_4$  ( $f=0.1923$ ), which is also LLCT in nature (HOMO $\rightarrow$ LUMO + 1, 94%). The  $T_1$  state is predominantly LLCT between Cz and IPrBIAN (HOMO $\rightarrow$ LUMO, 77%), although there is some contribution from an LC transition localized on the IPrBIAN ligand (HOMO-2 $\rightarrow$ LUMO, 22%).

The geometry of **3** at the lowest energy excited state ( $T_1$ ) was then optimized; its structure is broadly similar to the ground state structure, except for slightly shorter bond lengths to the copper center (Cu1–C1 and Cu1–N52 bond distances are 1.846 Å and 1.839 Å, respectively) and a reduction in the already small angle between the mean-planes of the IPrBIAN and Cz ligands to 2.52°. The spin density of the  $T_1$  state of **3** (Figure 6(b)) is distributed across both the IPrBIAN and Cz ligands, corroborating the LLCT nature of the triplet state determined by TD-DFT and consistent with the experimental results (*vide infra*). The calculated vertical emission from this triplet state is 822 nm.

### 3.4. UV-vis absorption properties

The UV-vis absorption spectra of **1H.Cl**, **2**, and **3** were recorded in DCM solution at room temperature (Figure 7(a)) and the data are summarized in Table 4. Overlays of experimental and calculated absorption spectra alongside predicted oscillator strengths for the associated vertical transitions of **3** are shown in Figure 7(b). Selected transitions from TDDFT calculations are summarized in Table 3.

The three compounds **1H.Cl**, **2**, and **3** all show a strong absorption band at 233–235 nm with  $\epsilon=23\text{--}27 \times 10^3 \text{ M}^{-1} \text{ cm}^{-1}$  and another between 279 and 292 nm with  $\epsilon=18\text{--}24 \times 10^3 \text{ M}^{-1} \text{ cm}^{-1}$ , both of which are characteristic of locally-excited

**Table 4.** Absorption data of **1H.Cl**, **2**, and **3** in DCM at room temperature.

Compound	$\lambda_{\text{abs}}$ (nm) ( $\epsilon \times 10^{-3}/\text{M}^{-1}\text{cm}^{-1}$ )
<b>1H.Cl</b>	233 (27.4), 282 (20.1), 320 (11.3)
<b>2</b>	233 (23.1), 292 (18.4), 388 (1.10), 426 (1.23)
<b>3</b>	235 (27.5), 279 (24.4), 310 (13.9), 326 (14.6), 335 (13.2), 341 (12.6), 375 (1.90), 420 (0.54)

transitions on the NHC, as predicted by TD-DFT (Table 3). Carbazole has a characteristic absorption spectrum with peaks at 266 and 290 nm [42]; however, these are largely obscured in the absorption spectrum of **3**, with only a peak attributed to a LC transition on carbazole observed as a shoulder at 310 nm. The transitions observed at 326 and 375 nm can both be assigned to predominantly  $^1\text{LLCT}$  transition from Cz to IPrBIAN (HOMO-5  $\rightarrow$  LUMO and HOMO  $\rightarrow$  LUMO + 1, respectively).

Both **2** and **3** show a broad, weak CT transition at 426 nm (**2**) and 420 nm (**3**). For **2**, this CT absorption band encompasses the first three transitions ( $S_1$ ,  $S_2$ , and  $S_3$ ); all have both Cu ( $d\pi$ )  $\rightarrow$  IPrBIAN ( $\pi^*$ ) MLCT and IPrBIAN LC character (Table 3). For **3**, this LC absorption band is assigned to the  $S_3$  transition, which is HOMO-2  $\rightarrow$  LUMO with a predicted absorption maximum of 425 nm. This transition is predominantly a singlet  $^1\text{LLCT}$  transition from Cz to IPrBIAN with a minor contribution from a singlet  $^1\text{MLCT}$  component involving Cu ( $d\pi$ )  $\rightarrow$  IPrBIAN ( $\pi^*$ ) (Table 3).

### 3.5. Electrochemical properties of **3**

The redox behavior of **3** in degassed DCM was assessed by CV and DPV, respectively, at room temperature (Figure 8). Complex **3** exhibited an irreversible oxidation at 0.60 V versus SCE (Figure 8(a)) based on the peak value from the DPV scan. Based on the DFT calculations, the oxidation wave is assigned to oxidation of the carbazolate; the  $E_{\text{ox}}^{\text{pa}}$  for carbazole is significantly anodically shifted at ca. 1.16 V versus SCE [43]. Indeed, this irreversible oxidation behavior is typical of such copper(I) carbazolate-containing complexes, with many literature examples also showing irreversible oxidation waves [11c]. For example, Cu(MAC\*)(Cz) complexes (MAC\* = N,N'-bis(diisopropylphenyl)-5,5-dimethyl-4-keto-tetrahydropyrimidin-2-ylidene) exhibit an irreversible oxidation wave at  $E_{\text{ox}}^{\text{pa}} = 0.56$  V (vs. SCE in MeCN), with the oxidation primarily centered on the carbazolate ligand [11c]. This oxidation potential is very similar to **3** and so similar electronic coupling is present. Both **1H.Cl** and **2** exhibit an irreversible reduction wave at  $E_{\text{red}}^{\text{pc}}$  of  $-1.3$  V versus SCE (Figure 8(b)). This reduction wave is also present in the CV and DPV of **3**, shifted anodically to  $E_{\text{red}}^{\text{pc}}$  of  $-1.2$  V versus SCE, indicating a slightly more facile reduction of the NHC in this complex.

### 3.6. Emission properties of **3**

Complex **3** exhibits interesting emission properties in solution. When **3** is photoexcited into the carbazolate LC band at 300 nm, structured LC emission from the carbazolate ligand was observed with  $\lambda_{\text{PL}}$  between 338 and 359 nm (Figure 9(a) and Table 5). The LC emission is solvent insensitive and for measurements in degassed toluene, THF, and DCM solutions, this was the only emission observed. In degassed chloroform, however, an additional emission band was observed with  $\lambda_{\text{PL}}$  of 539 nm. Based on

**Table 3.** Comparison of absorption data of 2 and 3 in DCM at room temperature with selected transitions from TD-DFT calculations of 2 and 3 in the singlet ground state (B3LYP/SBKJCV-DZ ECP[Cu]6–31G\*\*/[C,H,N], CPCM(CH<sub>2</sub>Cl<sub>2</sub>)).

State	$\epsilon \times 10^{-3} / \text{M}^{-1} \text{cm}^{-1}$ [expt.]	$\lambda_{\text{abs}}$ (nm) [TD-DFT]	$f$	Major transitions	Character
<b>COMPLEX 2</b>					
33	233 (23.1)	241	0.8770	H-2→L + 2	IPRBIAN ( $\pi^*$ ) LC (MAJOR)
13	292 (18.4)	298	0.6038	HOMO→L + 1 (80%)	IPRBIAN ( $\pi^*$ ) LC (MAJOR) + MLCT CU ( $D\pi$ ) TO IPRBIAN ( $\pi^*$ ) (MINOR)
3	388 (1.10)	384	0.3419	H-2→LUMO (97%)	IPRBIAN ( $\pi^*$ ) LC (MAJOR)
2	426 (1.23)	398	0.0002	H-1→LUMO (99%)	MLCT CU ( $D\pi$ ) TO IPRBIAN ( $\pi^*$ ) (MAJOR) + IPRBIAN ( $\pi^*$ ) LC (MINOR)
1	–	522	0.0223	HOMO→LUMO (97%)	IPRBIAN ( $\pi^*$ ) LC (MAJOR) + MLCT CU ( $D\pi$ ) TO IPRBIAN ( $\pi^*$ ) (MINOR)
<b>COMPLEX 3</b>					
48	235 (27.5)	241	0.0498	H-5→L + 1 (49%), H-4→L + 1 (19%)	CZ ( $\pi$ ) TO IPRBIAN ( $\pi^*$ ) (MAJOR) + MLCT CU ( $D\pi$ ) TO IPRBIAN ( $\pi^*$ ) (MINOR)
36	–	253	0.5361	H-1→L + 4 (17%), HOMO→L + 8 (53%)	CZ ( $\pi$ ) TO IPRBIAN ( $\pi^*$ ) (MAJOR) + MLCT CU ( $D\pi$ ) TO IPRBIAN ( $\pi^*$ ) (MINOR)
24	279 (24.4)	278	0.3670	H-2→L + 1 (86%), H-6→LUMO (98%)	CZ ( $\pi$ ) TO IPRBIAN ( $\pi^*$ ) (MINOR)
14	310 (13.9)	310	0.0044	H-5→LUMO (95%)	IPRBIAN ( $\pi^*$ ) LC
8	326 (14.6)	326	0.1629	HOMO→L + 1 (94%)	CZ ( $\pi$ ) TO IPRBIAN ( $\pi^*$ ) (MAJOR) + CU ( $D\pi$ ) TO IPRBIAN ( $\pi^*$ ) (MINOR)
4	375 (1.90)	374	0.1932	H-2→LUMO (96%)	CZ ( $\pi$ ) TO IPRBIAN ( $\pi^*$ ) (MAJOR) + CU ( $D\pi$ ) TO IPRBIAN ( $\pi^*$ ) (MINOR)
3	420 (0.54)	425	0.0142		CZ ( $\pi$ ) TO IPRBIAN ( $\pi^*$ ) (MAJOR) + CU ( $D\pi$ ) TO IPRBIAN ( $\pi^*$ ) (MINOR)
1	–	584	0.0015		CZ ( $\pi$ ) TO IPRBIAN ( $\pi^*$ ) (MAJOR) + CU ( $D\pi$ ) TO IPRBIAN ( $\pi^*$ ) (MINOR)



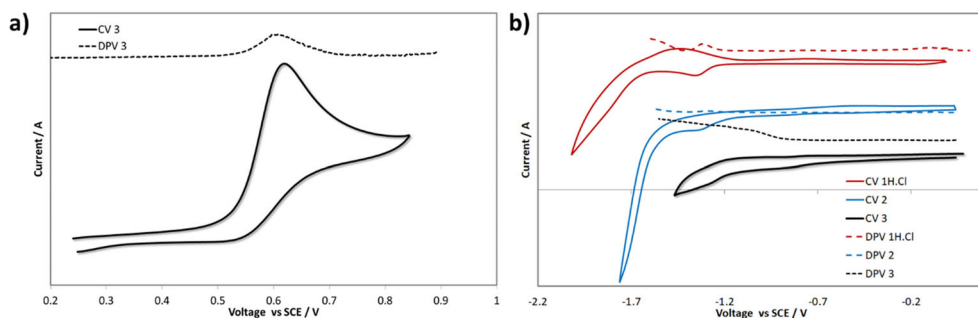


**Figure 8.** a) Cyclic voltammogram and DPV voltammogram of **3** in degassed DCM solution showing the first oxidation of **3**. b) Cyclic voltammogram and DPV voltammogram of **1H.Cl**, **2**, and **3** in degassed DCM solution showing the first reduction of **1H.Cl**, **2**, and **3**, respectively. Scan rate for CV:  $100 \text{ mV s}^{-1}$  in cathodic direction.

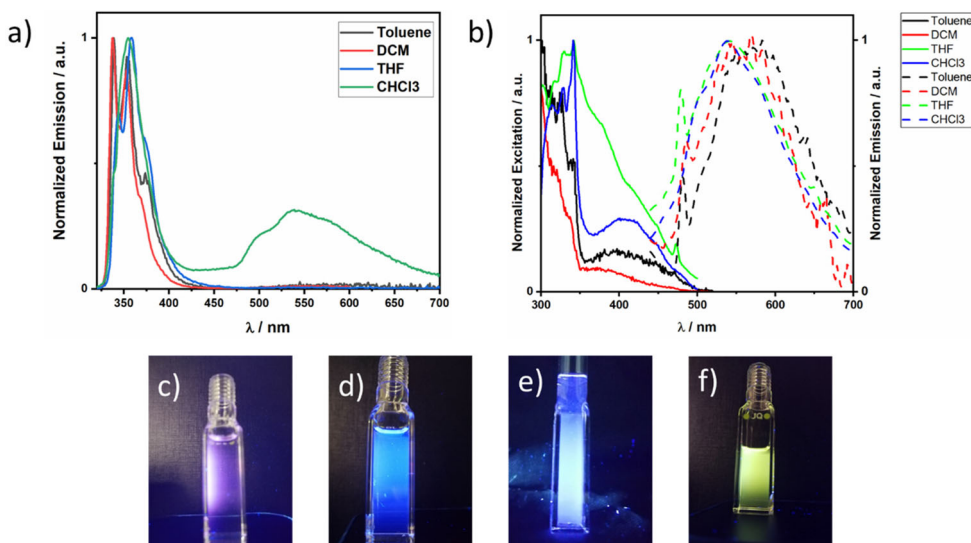


**Figure 9.** a) Normalized emission spectra of **3** in degassed solvents,  $\lambda_{\text{exc}} = 300 \text{ nm}$ . b) Normalized excitation (solid lines,  $\lambda_{\text{em}} = 550 \text{ nm}$ ) and emission (dashed lines,  $\lambda_{\text{exc}} = 420 \text{ nm}$ ) spectra of **3** in degassed solvents. Photos of emission from solutions of **3** when excited by UV torch at 365 nm in aerated solution of c) toluene, d) DCM, e) THF, and f) chloroform.

**Table 5.** Solution state emission data of **3** at 298 K.

Solvent	$\lambda_{\text{exc}} = 300 \text{ nm}$	$\lambda_{\text{exc}} = 420 \text{ nm}$
	$\lambda_{\text{PL}}/\text{nm}$	$\lambda_{\text{PL}}/\text{nm}$
Toluene	339, 353	583
DCM	338, 353	568
THF	344, 359	542
Chloroform	355, 539	539

DFT calculations, we assign this emission to originate from an LLCT state involving a Cz to IPrBIAN transition. Upon photoexcitation into the LLCT absorption band at 420 nm, emission from the LLCT state is observed in all solvents ( $\lambda_{\text{PL}}$  between 539 and 580 nm). In chloroform solution the energy of the LLCT emission remains unchanged

regardless of the excitation wavelength. The difference in emission behavior for **3** in different solvents is seen visually where the chloroform solution appears yellow/green, while the toluene, THF and DCM solutions present as violet to blue (Figure 9(c–f)). Excitation spectra were collected for all solutions, monitoring the LLCT emission ( $\lambda_{\text{em}} = 550\text{ nm}$ ). There exists a strong correlation between the absorption and excitation spectra, with strong excitation below 340 nm and a weaker low energy excitation band centered around 420 nm, indicating no photodegradation of the complex.

There is no delayed component to the emission, with all emission lifetimes for degassed chloroform solution in the ns range for both the LC emission [ $\lambda_{\text{em}} = 390\text{ nm}$ ,  $\tau = 1.64\text{ ns}$  (60%) and  $4.8\text{ ns}$  (40%)] and LLCT emission [ $\lambda_{\text{em}} = 550\text{ nm}$ ,  $\tau = 1.4\text{ ns}$  (75%) and  $7.4\text{ ns}$  (23%)]. The photoluminescence quantum yield for the very weak emission could not be accurately determined.

Dual emission has previously been observed for two-coordinate copper(I) carbazolate complexes. Cu(IPr)(Cz) shows dual emission in the crystalline powder state [13]; however, only carbazolate-based LC emission in THF solution ( $10\text{ }\mu\text{M}$ ) was observed, with a maximum at 342 and a shoulder at 378 nm. This is similar in both energy and structure to the LC emission that was observed for **3** in THF solutions ( $20\text{--}80\text{ }\mu\text{M}$ ) with a peak at 344 and shoulder at 359 nm. Recently, dual emission was reported for Cu(PyTz)(Cz) in THF solution, ascribed to a carbazolate-based LC state ( $\lambda_{\text{PL}} = 437\text{ nm}$ ) and an LLCT state ( $\lambda_{\text{PL}} = 594\text{ nm}$ ) [14]. It was proposed that the dual emission for Cu(PyTz)(Cz) was due to a mixture of conformers in solution, with LC emission originating from complexes with orthogonally disposed ligands and intermolecular LLCT resulting from through space interaction between ligands in  $\pi$ -stacked dimers of coplanar molecules. The use of a monomer-dimer equilibrium in solution to explain the dual emission was supported by DFT calculations on the copper complex and a series of concentration, temperature, and excitation energy studies on an analogous gold complex, Au(PyTz)(Cz). The origin of the solvent-specific dual emission of **3** in chloroform is presently unknown.

## 4. Conclusion

Two Cu(I)-NHC complexes, **2** and the novel two-coordinate **3**, both bearing the unusual NHC-BIAN ligand **1** were synthesized and characterized by various analytical techniques. Ligand **1** coordinates to Cu(I) as a neutral ligand to give **2**; further complexation with carbazole gave **3**. Both **2** and **3** show mixed LC transitions lower than 300 nm and weak LLCT transitions further into the visible region. Complex **3** exhibited interesting dual emission properties in solution; this is seen as separate emission depending on excitation source for most solvents, and is especially strong in chloroform solution, an interesting phenomenon that warrants further study. Although no delayed component was observed for the emission at room temperature, further investigation of this interesting emission is ongoing.

## Disclosure statement

No potential conflict of interest was reported by the authors.

## Funding

CFRM and EZ-C wish to thank the Engineering and Physical Sciences Research Council (EP/M02105X/1 and EP/R035164/1). We would like to thank the Engineering and Physical Sciences Research Council and CRITICAT Centre for Doctoral Training for financial support (Ph.D. studentship to B. H.; EP/L016419/1). CFRM and EZ-C wish to thank the Engineering and Physical Sciences Research Council (EP/M02105X/1 and EP/R035164/1) and CRITICAT Centre for Doctoral Training for financial support (Ph.D. studentship to B. H.; EP/L016419/1).

## ORCID

Bryony M. Hockin  <http://orcid.org/0000-0002-4687-3806>  
 Campbell F. R. Mackenzie  <http://orcid.org/0000-0001-7465-8989>  
 David B. Cordes  <http://orcid.org/0000-0002-5366-9168>  
 Alexandra M. Z. Slawin  <http://orcid.org/0000-0002-9527-6418>  
 Neil Robertson  <http://orcid.org/0000-0002-9230-6124>  
 Eli Zysman-Colman  <http://orcid.org/0000-0001-7183-6022>

## References

- [1] (a) B.M. Hockin, C. Li, N. Robertson, E. Zysman-Colman. *Catal. Sci. Technol.*, **9**, 889 (2019). (b) A. Hossain, A. Bhattacharyya, O. Reiser. *Science*, **364**, eaav9713 (2019). (c) C. Minozzi, A. Caron, J.C. Grenier-Petel, J. Santandrea, S.K. Collins. *Angew. Chem. Int. Ed.*, **57**, 5477 (2018).
- [2] (a) T. Hirayama, G.C. Van de Bittner, L.W. Gray, S. Lutsenko, C.J. Chang. *Proc. Natl. Acad. Sci. USA.*, **109**, 2228 (2012). (b) S. Jia, K.M. Ramos-Torres, S. Kolemen, C.M. Ackerman, C.J. Chang. *ACS Chem. Biol.*, **13**, 1844 (2018). (c) S. Lee, C.Y. Chung, P. Liu, L. Craciun, Y. Nishikawa, K.J. Brummer, I. Hamachi, K. Saijo, E.W. Miller, C.J. Chang. *J. Am. Chem. Soc.*, **142**, 14993 (2020).
- [3] (a) H. Xu, R. Chen, Q. Sun, W. Lai, Q. Su, W. Huang, X. Liu. *Chem. Soc. Rev.*, **43**, 3259 (2014). (b) F. Wei, J. Qiu, X. Liu, J. Wang, H. Wei, Z. Wang, Z. Liu, Z. Bian, Z. Lu, Y. Zhao, C. Huang. *J. Mater. Chem. C*, **2**, 6333 (2014). (c) M. Osawa, M. Hoshino, M. Hashimoto, I. Kawata, S. Igawa, M. Yashima. *Dalton Trans.*, **44**, 8369 (2015). (d) M. Hashimoto, S. Igawa, M. Yashima, I. Kawata, M. Hoshino, M. Osawa. *J. Am. Chem. Soc.*, **133**, 10348 (2011).
- [4] R. Czerwieniec, M.J. Leidl, H.H.H. Homeier, H. Yersin. *Coord. Chem. Rev.*, **325**, 2 (2016).
- [5] (a) M.W. Mara, K.A. Fransted, L.X. Chen. *Coord. Chem. Rev.*, **282–283**, 2 (2015). (b) M. Iwamura, H. Watanabe, K. Ishii, S. Takeuchi, T. Tahara. *J. Am. Chem. Soc.*, **133**, 7728 (2011). (c) N. Armaroli, G. Accorsi, F. Cardinali, A. Listorti, In *Photochemistry and Photophysics of Coordination Compounds I*, V. Balzani, S. Campagna (Eds.), pp. 69–115, Springer, Berlin, Heidelberg (2007). (d) G. Capano, M. Chergui, U. Rothlisberger, I. Tavernelli, T.J. Penfold. *J. Phys. Chem. A*, **118**, 9861 (2014).
- [6] (a) D.J. Gaspar, E. Polikarpov, *OLED Fundamentals: Materials, Devices, and Processing of Organic Light-Emitting Diodes*, CRC Press, Boca Raton, FL (2015). (b) C.E.A. Palmer, D.R. McMillin. *Inorg. Chem.*, **26**, 3837 (1987). (c) C.E.A. Palmer, D.R. McMillin, C. Kirmaier, D. Holten. *Inorg. Chem.*, **26**, 3167 (1987).
- [7] (a) J.C. Deaton, S.C. Switalski, D.Y. Kondakov, R.H. Young, T.D. Pawlik, D.J. Giesen, S.B. Harkins, A.J.M. Miller, S.F. Mickenberg, J.C. Peters. *J. Am. Chem. Soc.*, **132**, 9499 (2010). (b) R. Czerwieniec, J. Yu, H. Yersin. *Inorg. Chem.*, **50**, 8293 (2011). (c) C.L. Linfoot, M.J. Leidl, P. Richardson, A.F. Rausch, O. Chepelin, F.J. White, H. Yersin, N. Robertson. *Inorg. Chem.*, **53**, 10854 (2014). (d) D. Felder, J.F. Nierengarten, F. Barigelletti, B. Ventura, N. Armaroli. *J. Am. Chem. Soc.*, **123**, 6291 (2001). (e) C.E. McCusker, F.N. Castellano. *Inorg. Chem.*, **52**, 8114 (2013). (f) D.G. Cuttall, S. M. Kuang, P.E. Fanwick, D.R. McMillin, R.A. Walton. *J. Am. Chem.*

- Soc., **124**, 6 (2002). (g) N. Lin, J. Qiao, L. Duan, L. Wang, Y. Qiu. *J. Phys. Chem. C*, **118**, 7569 (2014). (h) A. Lavie-Cambot, M. Cantuel, Y. Leydet, G. Jonusauskas, D. Bassani, N. McClenaghan. *Coord. Chem. Rev.*, **252**, 2572 (2008).
- [8] K.J. Lotito, J.C. Peters. *Chem. Commun. (Camb.)*, **46**, 3690 (2010).
- [9] (a) V.A. Krylova, P.I. Djurovich, M.T. Whited, M.E. Thompson. *Chem. Commun. (Camb.)*, **46**, 6696 (2010). (b) V.A. Krylova, P.I. Djurovich, B.L. Conley, R. Haiges, M.T. Whited, T.J. Williams, M.E. Thompson. *Chem. Commun.*, **50**, 7176 (2014). (c) M. Gernert, U. Muller, M. Haehnel, J. Pflaum, A. Steffen. *Chem. Eur. J.*, **23**, 2206 (2017). (d) R. Molteni, K. Edkins, M. Haehnel, A. Steffen. *Organometallics*, **35**, 629 (2016). (e) M.D. Weber, E. Fresta, M. Elie, M.E. Miehlich, J.-L. Renaud, K. Meyer, S. Gaillard, R.D. Costa. *Adv. Funct. Mater.*, **28**, 1707423 (2018). (f) M.J. Leitl, V.A. Krylova, P.I. Djurovich, M.E. Thompson, H. Yersin. *J. Am. Chem. Soc.*, **136**, 16032 (2014). (g) S. Shi, P.I. Djurovich, M.E. Thompson. *Inorg. Chim. Acta*, **482**, 246 (2018). (h) B. Hupp, C. Schiller, C. Lenczyk, M. Stanoppi, K. Edkins, A. Lorbach, A. Steffen. *Inorg. Chem.*, **56**, 8996 (2017). (i) M. Elie, F. Sguerra, F. Di Meo, M.D. Weber, R. Marion, A. Grimault, J.F. Lohier, A. Stallivieri, A. Brosseau, R.B. Pansu, J.L. Renaud, M. Linares, M. Hamel, R.D. Costa, S. Gaillard. *ACS Appl. Mater. Interfaces*, **8**, 14678 (2016). (j) R. Marion, F. Sguerra, F. Di Meo, E. Sauvageot, J.F. Lohier, R. Daniellou, J.L. Renaud, M. Linares, M. Hamel, S. Gaillard. *Inorg. Chem.*, **53**, 9181 (2014).
- [10] K.A. Barakat, T.R. Cundari, M.A. Omary. *J. Am. Chem. Soc.*, **125**, 14228 (2003).
- [11] (a) R. Hamze, J.L. Peltier, D. Sylvinson, M. Jung, J. Cardenas, R. Haiges, M. Soleilhavoup, R. Jazzar, P.I. Djurovich, G. Bertrand, M.E. Thompson. *Science*, **363**, 601 (2019). (b) D. Di, A.S. Romanov, L. Yang, J.M. Richter, J.P.H. Rivett, S. Jones, T.H. Thomas, M. Abdi Jalebi, R.H. Friend, M. Linnolahti, M. Bochmann, D. Credgington. *Science*, **356**, 159 (2017). (c) S. Shi, M.C. Jung, C. Coburn, A. Tadler, M.R.D. Sylvinson, P.I. Djurovich, S.R. Forrest, M.E. Thompson. *J. Am. Chem. Soc.*, **141**, 3576 (2019). (d) M. Gernert, L. Balles-Wolf, F. Kerner, U. Müller, A. Schmiedel, M. Holzapfel, C.M. Marian, J. Pflaum, C. Lambert, A. Steffen. *J. Am. Chem. Soc.*, **142**, 8897 (2020).
- [12] Y. Zhang, M. Schulz, M. Wächtler, M. Karnahl, B. Dietzek. *Coord. Chem. Rev.*, **356**, 127 (2018).
- [13] J. Li, L. Wang, Z. Zhao, X. Li, X. Yu, P. Huo, Q. Jin, Z. Liu, Z. Bian, C. Huang. *Angew. Chem. Int. Ed. Engl.*, **59**, 8210 (2020).
- [14] L. Cao, S. Huang, W. Liu, H. Zhao, X.G. Xiong, J.P. Zhang, L.M. Fu, X. Yan. *Chem. Eur. J.*, **26**, 17222 (2020).
- [15] R.R. Butorac, S.S. Al-Deyab, A.H. Cowley. *Molecules*, **16**, 2285 (2011).
- [16] (a) W. Fang, Q. Deng, M. Xu, T. Tu. *Org. Lett.*, **15**, 3678 (2013). (b) T. Tu, Z. Sun, W. Fang, M. Xu, Y. Zhou. *Org. Lett.*, **14**, 4250 (2012). (c) Z. Liu, N. Dong, M. Xu, Z. Sun, T. Tu. *J. Org. Chem.*, **78**, 7436 (2013).
- [17] K.V. Vasudevan, R.R. Butorac, C.D. Abernethy, A.H. Cowley. *Dalton Trans.*, **39**, 7401 (2010).
- [18] E. Merino, E. Poli, U. Díaz, D. Brunel. *Dalton Trans.*, **41**, 10913 (2012).
- [19] N.G. Connelly, W.E. Geiger. *Chem. Rev.*, **96**, 877 (1996).
- [20] CrystalClear-SM Expert v2.1, *Rigaku Americas and Rigaku Corporation*, The Woodlands, TX and Tokyo, Japan (2015).
- [21] Rigaku Oxford Diffraction. *CrysAlisPro*, Rigaku Corporation, Oxford (2015).
- [22] M.C. Burla, R. Caliendo, M. Camalli, B. Carrozzini, G.L. Casciaro, L. De Caro, C. Giacovazzo, G. Polidori, R. Spagna. *J. Appl. Crystallogr.*, **38**, 381 (2005).
- [23] G.M. Sheldrick. *Acta Crystallogr. A Found Adv.*, **71**, 3 (2015).
- [24] G.M. Sheldrick. *Acta Crystallogr. C Struct. Chem.*, **71**, 3 (2015).
- [25] A.L. Spek. *Acta Crystallogr. C Struct. Chem.*, **71**, 9 (2015).
- [26] A.L. Spek. *Acta Crystallogr. D Biol. Crystallogr.*, **65**, 148 (2009).
- [27] CrystalStructure v4.3.0. *Rigaku Americas and Rigaku Corporation*, The Woodlands, TX and Tokyo, Japan (2018).
- [28] C. O'Brien, M.Y. Wong, D.B. Cordes, A.M.Z. Slawin, E. Zysman-Colman. *Organometallics*, **34**, 13 (2015).

- [29] M.J.; Frisch, G.W.; Trucks, H.B.; Schlegel, G.E.; Scuseria, M.A.; Robb, J.R.; Cheeseman, G.; Scalmani, V.; Barone, B.; Mennucci, G.A.; Petersson, H.; Nakatsuji, M.; Caricato, X.; Li, H.P.; Hratchian, A.F.; Izmaylov, J.; Bloino, G.; Zheng, J.L.; Sonnenberg, M.; Hada, M.; Ehara, K.; Toyota, R.; Fukuda, J.; Hasegawa, M.; Ishida, T.; Nakajima, Y.; Honda, O.; Kitao, H.; Nakai, T.; Vreven, J.A.; Montgomery, J.E.; Peralta, F.; Ogliaro, M.; Bearpark, J.J.; Heyd, E.; Brothers, K.N.; Kudin, V.N.; Staroverov, R.; Kobayashi, J.; Normand, K.; Raghavachari, A.; Rendell, J.C.; Burant, S.S.; Iyengar, J.; Tomasi, M.; Cossi, N.; Rega, J.M.; Millam, M.; Klene, J.E.; Knox, J.B.; Cross, V.; Bakken, C.; Adamo, J.; Jaramillo, R.; Gomperts, R.E.; Stratmann, O.; Yazyev, A.J.; Austin, R.; Cammi, C.; Pomelli, J.W.; Ochterski, R.L.; Martin, K.; Morokuma, V.G.; Zakrzewski, G.A.; Voth, P.; Salvador, J.J.; Dannenberg, S.; Dapprich, A.D.; Daniels, O.; Farkas, J.B.; Foresman, J.V.; Ortiz, J.; Cioslowski, D.J.; Fox. *Gaussian 09, Revision D.01*, Gaussian, Inc., Wallingford, CT (2009).
- [30] (a) A.D. Becke. *J. Chem. Phys.*, **98**, 5648 (1993). (b) C. Lee, W. Yang, R.G. Parr. *Phys. Rev. B: Condens. Matter*, **37**, 785 (1988).
- [31] A.D. McLean, G.S. Chandler. *J. Chem. Phys.*, **72**, 5639 (1980).
- [32] W.J. Stevens, M. Krauss, H. Basch, P.G. Jasien. *Can. J. Chem.*, **70**, 612 (1992).
- [33] (a) M. Cossi, N. Rega, G. Scalmani, V. Barone. *J. Comput. Chem.*, **24**, 669 (2003). (b) M. Cossi, V. Barone. *J. Chem. Phys.*, **115**, 4708 (2001). (c) V. Barone, M. Cossi. *J. Phys. Chem. A*, **102**, 1995 (1998).
- [34] (a) M.E. Casida, C. Jamorski, K.C. Casida, D.R. Salahub. *J. Chem. Phys.*, **108**, 4439 (1998). (b) R.E. Stratmann, G.E. Scuseria, M.J. Frisch. *J. Chem. Phys.*, **109**, 8218 (1998).
- [35] R. Dennington, T. Keith, J. Millam. *Gaussview 5.0*, Semichem Inc., Shawnee Mission, KS (2009).
- [36] L. Skripnikov. *Chemissian v4.67*, Lenoid Skripnikov, St. Petersburg, Russia (2020).
- [37] N.M. O'Boyle, A.L. Tenderholt, K.M. Langner. *J. Comput. Chem.*, **29**, 839 (2008).
- [38] (a) K. Hasan, E. Zysman-Colman. *J. Phys. Org. Chem.*, **26**, 274 (2013). (b) Z. Balzadeh, H. Arabi. *React. Funct. Polym.*, **111**, 68 (2017).
- [39] R.R. Butorac, S.S. Al-Deyab, A.H. Cowley. *Molecules*, **16**, 3168 (2011).
- [40] (a) V.W.W. Yam, J.K.W. Lee, C.C. Ko, N. Zhu. *J. Am. Chem. Soc.*, **131**, 912 (2009). (b) H.M.J. Wang, C.S. Vasam, T.Y.R. Tsai, S.H. Chen, A.H.H. Chang, I.J.B. Lin. *Organometallics*, **24**, 486 (2005).
- [41] M. Mamada, K. Inada, T. Komino, W.J. Potscavage, Jr., H. Nakanotani, C. Adachi. *ACS Cent. Sci.*, **3**, 769 (2017).
- [42] S. Jana, F. He, R.M. Koenigs. *Org. Lett.*, **22**, 4873 (2020).
- [43] K. Karon, M. Lapkowski. *J. Solid State Electrochem.*, **19**, 2601 (2015).